Thermochimica Acta 517 (2011) 9–15

Contents lists available at ScienceDirect

Thermochimica Acta

journal homepage: www.elsevier.com/locate/tca

Curing behavior and structure of a novel nanocomposite from glycerol diglycidyl ether and 3,3-dimethylglutaric anhydride

Abdollah omrani[a,*], Abbas Ali Rostami[a], Fatemeh Ravari[a], Arezu Mashak[b]

[a] Faculty of chemistry, University of Mazandaran, P.O. Box 453, Babolsar, Iran
[b] Iran Polymer and Petrochemical Institute, P.O. Box 14965-115, Tehran, Iran

ARTICLE INFO

Article history:
Received 5 November 2010
Received in revised form 8 January 2011
Accepted 13 January 2011
Available online 3 March 2011

Keywords:
Glycerol diglycidyl ether
Thermoset nanocomposite
DSC
Morphology

ABSTRACT

A novel nanocomposite was synthesized by curing of glycerol diglycidyl ether (GDE) and 3,3-dimethylglutaric anhydride (DGA) in the presence of alumina nanoparticles. Kinetics of GDE/DGA/nano-Al_2O_3 cure was studied by DSC measurements at dynamic and isothermal states. It was shown that the reaction kinetics could be described well by the Horie model. The advanced isoconversional method developed by Vyazovkin is utilized to describe the curing behavior of the nanocomposite. A technique of predicting isothermal cure time from the sole dependence of E_a on α was then considered and compared to the experimental results. The structure of the nanocomposite was characterized by X-ray diffraction analysis and scanning electron microscopy imaging. The SEM images showed that the nanocomposite has the morphology of homogeneous dispersion of alumina nanoparticles. It was shown by TGA measurements that the incorporation of nano-Al_2O_3 into GDE/DGA matrix results in thermal resistance improvement.

1. Introduction

Epoxy resins are the most important class of thermosetting polymers that widely used as matrices in reinforced composites, adhesives in the aerospace industry, and surface coatings [1]. These resins have good thermal, electrical and mechanical properties, but they are brittle and have poor resistance to crack propagation [2]. Epoxy resins could be polymerized in the presence of amine and anhydride reagents. Anhydride curing agents were used in the most important applications of epoxy resins, particularly in casting and laminates. Anhydride cured epoxies provide a lower exotherm during cure and generally give better thermal stability, electrical insulation, and transparency [3,4]. They are less poisonous, absorb less water, and undergo cure shrinkage [5]. On the other hand, non-catalyzed epoxy-anhydride mixtures are very low reactive and the curing reaction should be carried out at higher temperatures. So, the anhydride ring must first be opened by a compound having active hydrogen such as water and hydroxyl compounds. The use of a dispersed second phase in epoxy resin [6–14] serves two main purposes: (1) to reduce the cost of a component by incorporating reasonable percentage of low-cost material and (2) to impart some desired property to the system. Various inert and active organic and inorganic fillers at micro and nano scales were used to produce reinforced composites. Metal nanoparticles exhibit novel physical and chemical properties due to their small size, surface, quantum size and quanta tunnel effects. Nanoalumina is an enormously important engineering material due to compact crystal structure, excellent mechanical strength, highly thermal and chemical stability [15,16]. For the epoxy based composites, a good model enables to predict how the system will behave during cure. The most important component of such a model is a description of the kinetics of cure.

By starting a series of studies, our final aim is to design new nanocomposites based on low viscous diglycidyl ethers cured with various anhydrides which are useful in electronic industry with improved arc and track resistances. As it was necessary to synthesis the samples for electrical properties assessments at optimum conditions, the present work was aimed at studying the cure kinetics, thermal, and morphological properties of glycerol diglycidyl ether (GDE)/3,3-dimethylglutaric anhydride (DGA) system reinforced with alumina nanoparticles. Study on electrical properties of the produced nanocomposites using electrochemical impedance spectroscopy (EIS) technique is out of scope of the present paper and it will be presented as an independent work in the future. However, depending on the curing temperature, time, and formulation of the compositions for a same system, it is possible to obtain different thermal, mechanical, and electrical properties of the macromolecular structure at the end of the polymerization. Cure kinetics models are generally progressed by analysing experimental results obtained by differential scanning calorimetry (DSC) [17–19]. The DSC technique was extensively used for several applications in various industries and in determination of reaction

* Corresponding author. Tel.: +98 11252 42025; fax: +98 11252 42002.
E-mail address: omrani@umz.ac.ir (A. omrani).

0040-6031/$ – see front matter © 2011 Elsevier B.V. All rights reserved.
doi:10.1016/j.tca.2011.01.024

kinetics, degree of crystallinity, melting point and glass transition temperature of polymers and nanocomposites.

2. Experimental

2.1. Materials

Glycerol diglycidyl ether (GDE), molecular weight 204.22 g/mol, and alumina nanoparticles with an average size of 50 nm were purchased from Aldrich chemical company (Germany). The purity of as received nanoalumina is greater than 95%. The hardener was 3,3-dimethylglutaric anhydride (DGA) having molecular weight of 142.15 g/mol was obtained from A Johnson Matthey Ltd. (Germany). Triethylamine (TEA) was purchased from Merck and used as initiator. The materials were used without further treatments.

2.2. Sample preparation and optimum formulation

Glycerol diglycidyl ether (1 g) is added to the anhydride curing agent at stoichiometric ratio ($X_{ep} = 0.33$, that X_{ep} is epoxy molar ratio.) and then fixed amount of nano-Al_2O_3 sol (i.e., 1, 2.5, 5, 10, and 15 phr) was incorporated into the above mixture. The mixtures were further homogenized by ultrasonic treatment for a period of 2 h at room temperature. In the final stage, the initiator was added at $X_{TEA} = 0.0188$ (respect to the total mass of the epoxy and anhydride) and ultrasonicated for additional 5 min. To determine the optimum composition, the effect of nano-Al_2O_3 content on the reaction enthalpy was investigated by calorimetry measurements. Accordingly, 10% level of nano-Al_2O_3 loading was found to be the best composition as the result of maximum reaction heat.

2.3. Characterizations

DSC measurements were performed on a Perkin Elmer DSC-7 differential scanning calorimeter in dry nitrogen atmosphere (flow rate of 50 ml/min). The calorimeter was calibrated using high purity indium. Samples were placed in the hermetically aluminum pan, weighted around 14 mg, and then covered by an aluminum lid prior to undergoes a specific cure program depend on the mode of measurement. Dynamic DSC scans were conducted in the temperature rang of 25–280 °C at five different heating rates of 2.5, 5, 7.5, 10 and 15 °C/min. Isothermal experiments were carried out at 110, 120, 130 and 140 °C in this work. The glass transition temperature (T_g) of the cured sample was measured based on the second scan.

The structures of the neat GDE system and its nanocomposite were analysed by a Philips advance powder X-ray diffractometer (XRD) with Cu K_α radiation source ($\lambda = 0.1542$ nm) and a curved graphite crystal monochromator under 40 kV and 50 mA conditions. The scanning rate was 2°/min.

Also, to observe the phase structure of the cured materials, the samples were fractured under cryogenic condition using liquid nitrogen. The fracture surfaces were coated with thin layers of gold of about 100 Å. All specimens were characterized for the surface morphology and superficial elemental composition at some points of interest, using a scanning electron microscope (SEM) (VEGA Company TESCAN).

Thermal stability of the neat GDE system and GDE nanocomposite was examined by a thermogravimetric analyzer (TGA) on a Polymer Lab TGA-1500 (London, UK) ramped at 10 °C/min from 25 to 700 °C under nitrogen. The flow rates were maintained at 10 and 90 ml/min for the balance part and for the furnace area, respectively.

3. Results and discussion

3.1. Calorimetry study

To select suitable temperatures for the isothermal experiments, a dynamic DSC scan at 7.5 °C/min was obtained. Temperatures above but near to the onset of curing reaction were chosen as isothermal curing temperatures. Accordingly, isothermal calorimetry experiments were conducted at 110, 120, 130 and 140 °C.

Fig. 1 shows DSC curves recorded at various curing temperatures. Clearly, the maximum rate of the cure exotherm was increased by raising isothermal temperature while the time to reach the maximum is decreased.

The total reaction heat values (obtained by integration of the area between the peaks and the baseline), are in the range of 155.2–228.1 J/g; this fact shows that it is strongly depend on the selected curing temperature. Moreover this confirms that the temperature induces significant effects on the final properties of the cured samples for this system. Our results showed that the reaction heat was increased about 47% while the curing time decreased 5.2 times by increasing the isothermal temperature from 110 to 140 °C. This could be interpreted based on an increase in the reaction rate with temperature. Curves of conversion rate vs. conversion were also obtained by numerically integrating of the heat flow curves and then scaled by the total reaction enthalpy. These curves were shown in Fig. 2. As expected, the reaction rate is promoted by selecting greater values of isothermal curing temperature.

To get an idea about the glass transition temperature the isothermally cured sample at 130 °C was cooled to −30 °C and reheated at 5 °C/min–200 °C. The value of T_g, was obtained around 20 °C.

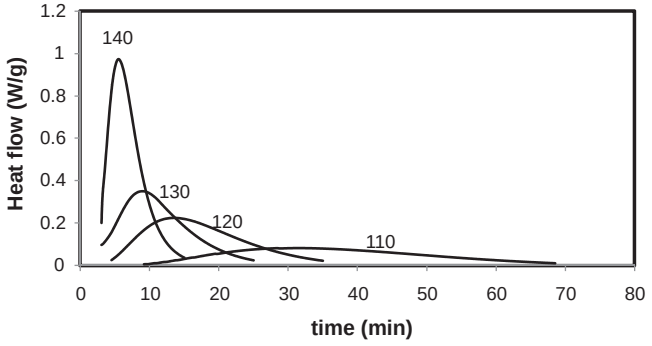

Fig. 1. DSC curves of the GDE/DGA/nanoalumina system at various isothermal temperatures.

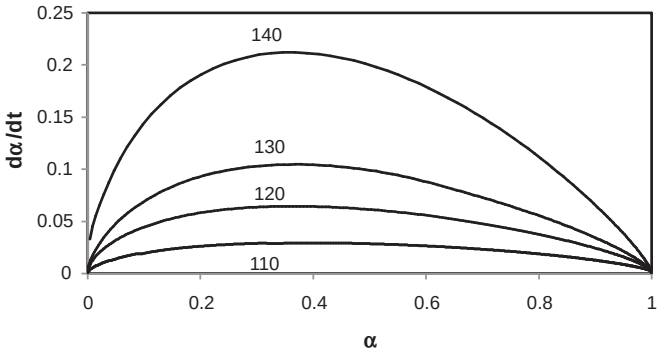

Fig. 2. Reaction rate as a function of conversion at various temperatures.

Table 1
Values of k_1, k_2, m and n evaluated using the Kamal model.

Temperature(°C)	k_1	k_2	m	n	$(m+n)$	E_1 (kJ/mol)	E_2 (kJ/mol)
110	0.0002	0.0615	0.556	0.582	1.138		
120	0.0012	0.1252	0.508	0.611	1.119	221.920	82.284
130	0.0057	0.1625	0.473	0.608	1.081		
140	0.0331	0.4566	0.642	0.729	1.371		

3.2. Model of cure kinetics in isothermal mode

The kinetic analysis in the present research is based on the assumption that the heat generated during the curing reaction is equal to the total area under the heat flow-time curve. Over the past decades, a lot of studies suggested that the curing process of epoxy systems involve multiple steps with different activation energies in various stages. Therefore, more complex models such as Kamal's equation are recognized to be suitable to model cure kinetics at isothermal mode [20–27]. The Kamal autocatalytic kinetics was expressed according to the following equation:

$$\frac{d\alpha}{dt} = (k_1 + k_2\alpha^m)(1-\alpha)^n \quad (1)$$

where, α is the conversion, k_1 and k_2 are the rate constants, m and n are the reaction orders of the autocatalytic and n-order reactions, respectively. The constant k_1 can be graphically estimated as the initial reaction rate at $t = 0$. Based on the curves in Fig. 1 and using the Kamal model, the kinetics parameters were calculated by a graphical method [25] and the results presented in Table 1. Also, the overall reaction order is known to be 2 in the case of epoxy/amine system but its value changes between 1 and 1.4 for the selected system. Obviously, the k_1 and k_2 values were increased with increasing curing temperature.

From the plot of the rate constants against temperature (based on the Arrhenius plot) straight lines were produced where the activation energies for the n-order and autocatalytic mechanism were estimated and listed in Table 1. The calculated kinetic parameters were used to predict curing behavior of the system at various isothermal temperatures. A typical comparison of the experimental data to those predicted by the model was shown in Fig. 3. Accordingly, the agreement between the two series data, i.e., experimental and predicted, is reasonable confirming suitability of the Kamal model to interpret GDE/DGA/nano-Al_2O_3 cure.

We have also examined our experimental data to the Horie model [17,28] which describes based on the following equation (by assuming $m = 1$):

$$\frac{d\alpha}{dt} = (k_1 + k_2\alpha)(1-\alpha)^n \quad (2)$$

The introduction of the variable exponent of n, an adjustable parameter, allows obtaining the best fitting of the experimental data. To obtain the best value of n, the Horie equation was presented in the following form:

$$\alpha^0 = \frac{(d\alpha/dt)}{(1-\alpha)^n} = k_1 + k_2\alpha \quad (3)$$

where, α^0 is defined as reduced rate. Different values of n among 0.1–2 were checked to obtain the best linear fitting of the experimental results. Our observations showed that the best fitting is corresponding to the $n = 1$ at all the isothermal temperatures. Once this value is found, it could be concluded that the overall reaction order $(m+n)$ is 2. Table 2 exhibits the rate constants corresponding to the n-order and autocatalytic mechanisms at various temperatures. The activation energies corresponding to the two kinetic mechanisms have also been obtained from the Arrhenius plots of $\ln k$ vs. $1/T$ and the results are presented in Table 2.

Table 2
Values of k_1, k_2, and E_a evaluated using the Horie model.

Temperature (°C)	k_1 (n-order)	k_2 (autocatalytic)	k_2/k_1	E_a (kJ/mol)	
				n-order	Autocatalytic
110	0.008	0.102	13.75		
120	0.018	0.218	12.11	100.96	75.67
130	0.027	0.322	11.92		
140	0.091	0.609	6.69		

To compare the applicability of the examined model to describe curing behavior of GDE/DGA/nanoalumina system, we introduced reaction rate vs. time plots. The kinetic parameters obtained above were used to compute the theoretical curves shown in Fig. 4 and compared to the experimentally obtained results.

From the graphs shown in Figs. 3 and 4, it can be seen that while the calculated time–reaction rate relationships using the Horie model are in better agreement to the experimental data, but the fitting becomes more reasonable by increasing the isothermal temperatures in the both cases. In other words, the disparity was greater at the lower temperatures used. Evidently, the both models were not able to completely describe the curing process of the GDE/DGA/nano-Al_2O_3 system, particularly at low curing temperatures. In conclusion, we implied that the Horie model is the better choice than the Kamal equation to interpret GDE/DGA/nano-Al_2O_3 cure.

We also produced the model E_a against conversion dependence plots using the following equation:

$$E_a = \frac{-Rd\ln(d\alpha/dt)_\alpha}{dT^{-1}} \quad (4)$$

The results were shown in Fig. 5. Solid circles in the Figure are the experimental data which determined by Eq. (4). Models (1) and

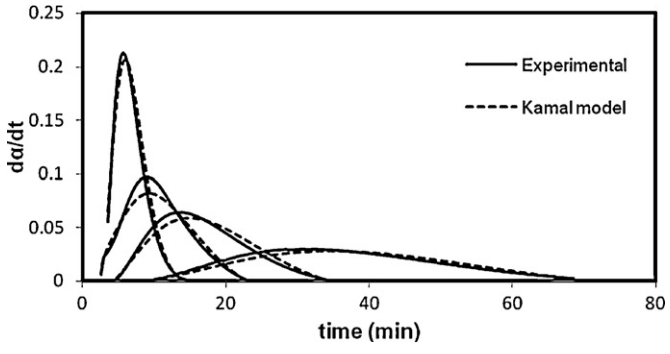

Fig. 3. Comparison of the experimental reaction rate with the predicted values using the Kamal model at various temperatures.

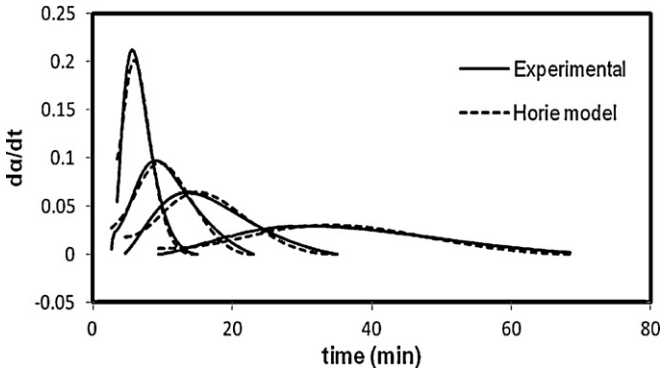

Fig. 4. Comparison of the experimental reaction rate with the predicted values using the Horie model at various temperatures.

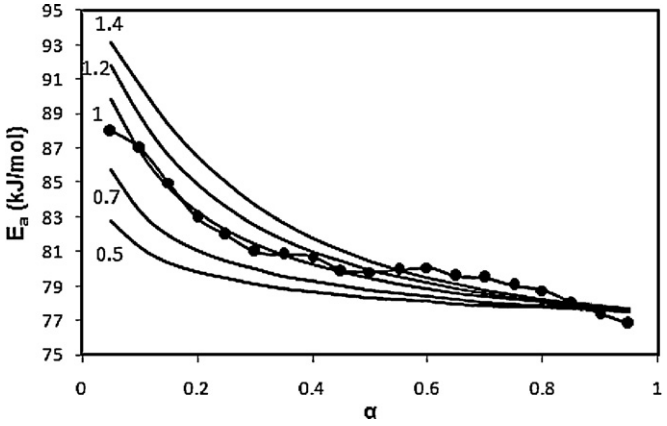

Fig. 5. Dependence of the activation energy upon conversion, experimental data (solid circle) and theoretical values for different m (solid line).

(2) can be utilized to further interpret the dependence of E_a on α. With respect to (4), E_a can be found from model (1) as

$$E_a = \frac{-Rd\ln[(k_1+\alpha^m k_2)(1-\alpha)^n]}{dT^{-1}} = \frac{(k_1E_1+\alpha^m k_2E_2)}{(k_1+\alpha^m k_2)} \quad (5)$$

and from model (2) as

$$E_a = \frac{-Rd\ln[(k_1+\alpha k_2)(1-\alpha)^n]}{dT^{-1}} = \frac{(k_1E_1+\alpha k_2E_2)}{(k_1+\alpha k_2)} \quad (6)$$

To fit our experimental data (solid circles), the numerical value of m in the above equations was changed (Fig. 5) from 0.5 to 1.4 [29].

The numerical values shown on each plot in Fig. 5 corresponds to an arbitrary value of m. The initial value of m was fixed at 0.5 since we obtained this amount of m using the kamal model. Interestingly, the best fitting of the experimental data was achieved by $m = 1$. Clearly, this value of m corresponds to the Horie model. Therefore, we concluded that the best model describing the curing behavior of the selected system is the Horie equation.

We also attempted to investigate the contribution of the n-order and autocatalytic pathways to the overall curing reaction by comparing the ratio of the rate constants calculated by the Horie model at various temperatures. Curing reaction of GDE/DGA/nano-Al_2O_3 system tends to proceed through n-order mechanism with increasing curing temperature (see Table 2). Clearly, as the isothermal temperature increased the contribution of n-order mechanism becomes significant and is comparable to the autocatalytic path.

3.3. Describe of the curing behavior using isoconversional methods

The isoconversional methods permit the effective activation energy of a thermal process to be unambiguously calculated as a function of the reaction progress. Analysis of the resulting E_a dependence could provide important clues about changes in the reaction mechanism if these changes could be associated with the variations in activation energy. Therefore, additional kinetic information may be obtained using special techniques [30] for estimating the pre-exponential factor whose value is also expected to vary with the extent of conversion.

3.3.1. The Flynn–Wall–Ozawa method

The isoconversional integral method proposed by Flynn, Wall, and Ozawa [31,32] was applied to the experimental data. Accordingly, the following equation was used:

$$\ln\ \beta = \ln\left(\frac{AE_a}{R}\right) - \ln g(\alpha) - 5.331 - 1.052\left(\frac{E_a}{RT}\right) \quad (7)$$

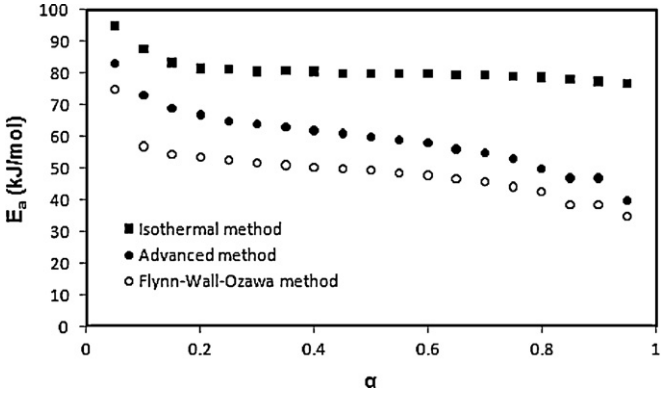

Fig. 6. Values of the activation energy obtained from Flynn–Wall–Ozawa, advanced isoconversional and isothermal isoconversional methods at different conversions.

$$g(\alpha) = \int_0^\alpha \frac{d\alpha}{f(\alpha)} \quad (8)$$

where, $g(\alpha)$ is a conversion dependence function. For a selected constant α, the plot of $(\ln \beta)$ against $(1/T)$ was introduced at various heating rates resulting in straight lines where the slope allows to find the activation energy. From the DSC data and applying the Eq. (7), we have calculated the activation energy for each conversion level as presented in Fig. 6. The results showed that the activation energy decreases by increasing of conversion. It can be seen that the activation energies remains almost constant during the propagation step of the curing reaction and an average value of about 50.44 kJ may be considered as effective activation energy. Apparently, by the progress of the curing reaction, the activation energy was decreased. Such a behavior is also reported by other researches on epoxy-amine cure [29,33].

3.3.2. Advanced isoconversional method

An advanced isoconversional method described by Vyazovkin [34–37] is an effective way to detect the complexity of the curing reaction and further evaluating the activation energy as a function of the epoxide conversion. In the present study, nonlinear isoconversional method was applied to the dynamic DSC data of GDE/DGA/nano-Al_2O_3 system using the following equation:

$$\Phi(E_a) = \sum_{i=1}^{n}\sum_{j\neq i}^{n}\frac{I(E_a, T_{a,i})\beta_j}{I(E_a, T_{a,j})\beta_i} \quad (9)$$

where, β is the heating rate, T is the temperature, E_a is the activation energy, i, j are the ordinal numbers of DSC runs performed at different heating rates. The activation energy can be find at any particular conversion level by finding the value of E_a at which the $\Phi(t)$ function has a minimum value. In Eq. (9) the temperature integral

$$I(E_a, T) = \int_0^{T\alpha} \exp\left(\frac{E_a}{RT}\right) dT \quad (10)$$

is determined by the Senum–Yang approximation [38]:

$$I(E_a, T) = \left(\frac{E_a}{R}\right) P(x) \quad (11)$$

and

$$P(x) = \frac{\exp(-x)}{x} \times \frac{\left(x^3+18x^2+88x+96\right)}{\left(x^4+20x^3+120x^2+240x+120\right)} \quad (12)$$

The minimization procedure is repeated for each value of α to determine the E_a-dependence. The advantage of the advanced

isoconversional method is that it applies the same computational algorithm to both isothermal and non-isothermal DSC data. Fig. 6 shows the isoconversional plot on our data. Clearly, a same trend to that obtained from Flynn–Wall–Ozawa method was observed. Also, Fig. 5 shows that the activation energy increased at $\alpha < 0.2$, it is approximately constant in the range of $0.2 < \alpha < 0.5$, and finally reduced. Anyways, the value of activation energy ranged from 40 to 100 kJ/mol. Some contribution from the autocatalytic nature of epoxy cure may be responsible to reduce the activation energy.

3.3.3. Isoconversional method of isothermal data

For isothermal conditions, the following equation was used [36] to find E_a vs. conversion dependence:

$$-\ln\ t_{\alpha,i} = \ln\left[\frac{A_\alpha}{g(\alpha)}\right] - \frac{E_a}{RT_i} \tag{13}$$

where $g(\alpha) = \int_0^\alpha [f(\alpha)]^{-1} d\alpha$ is the integral form of the reaction model, and $t_{a,i}$ is the time required to reach a specified conversion, α at temperature, T_i. In Eq. (13), E_a is evaluated from the slope of the plot $-\ln t_{\alpha,i}$ vs. $1/T_i$. The application of Eq. (13) to isothermal data, gives rise to decreasing of E_a on α (Fig. 6). It is worthy to note that the average value of E_a from isothermal data, about 85 kJ/mol, is in reliable agreement to those values of the activation energies determined by the Horie model (between 75 and 101 kJ/mol).

To illustrate a correlation between the values of activation energies obtained by the isoconversional isothermal method and those values predicted by models (1) and (2), E_a vs. conversion plots were produced using the kinetics parameters (in Tables 1 and 2) and Eqs. (5) and (6). The results were depicted in Fig. 7. Obviously, the E_a is not constant as expected. Significant changes observed for the E_1 and E_2 values, especially for the Kamal model, cannot be described by the isoconversional analysis of the isothermal data.

The main conclusion which can be driven from the kinetic analysis section is that fitting of GDE/DGA/nano-Al_2O_3 cure using the Kamal model has not allowed us to obtain the values of the activation energy that agree with those determined by the isothermal and non-isothermal isoconversional methods owing to unsuitability of the model fitting approaches to interpret epoxy cure.

3.4. Prediction

There have been various methods in the literatures in modeling of isothermal cure characteristics of a substance from non-isothermal data. We have employed the technique reported previously [35,39] to predict isothermal times of GDE/DGA/nano-Al_2O_3 cure using the data from dynamic calorimetery. Accordingly,

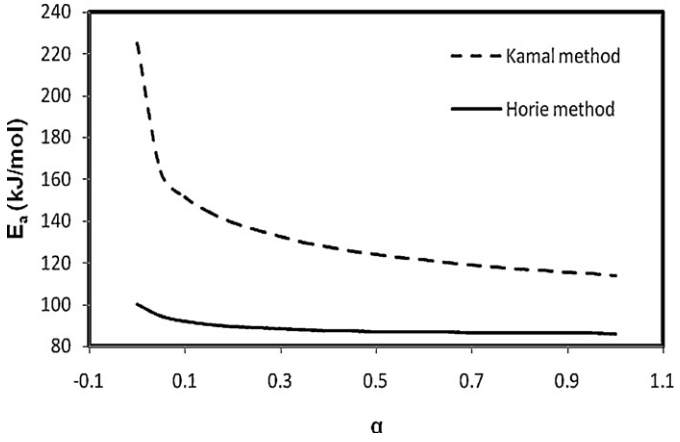

Fig. 7. Dependence of he activation energy upon conversion using the calculated kinetic parameters for models (1) and (2).

Table 3
The average values of the predicted and measured times to reach practically complete cure at different heating rates.

System	Measured time (min)	Predicted time (min) model	
		FWO	Advanced
110	56.6	30.23	35.76
120	27.6	22.89	25.98
130	18.1	17.58	19.17
140	10.5	13.67	14.36

the dynamic DSC data was treated by the following equation:

$$t_\alpha = \left[\beta \exp\left(\frac{-E_a}{RT_0}\right)\right]^{-1} \int_0^{T_\alpha} \exp\left(\frac{-E_a}{RT}\right) dT \tag{14}$$

This equation enables to calculate the time (t_α) at a given conversion for an arbitrary isothermal system with temperature, T_0. The time was calculated to reach 95% conversion at 110, 120, 130 and 140 °C. The value of activation energy that used for the calculation was obtained from Flynn–Wall–Ozawa and advanced isoconversional methods at $\alpha = 0.95$. Average values of the predicted times at different heating rates were calculated and compared to the experimental times in Table 3. Results from this Table indicated that there are better agreements between the theoretical and experimental values at higher isothermal temperatures.

3.5. Microstructure of the cured samples

XRD analysis was used to characterize the crystallographic structure of nanoalumina and the quality of its dispersion in glycerol diglycidyl ether matrix. XRD spectra of the pure nanoalumina (dashed line) and various GDE nanocomposites were shown in Fig. 8. The existence of various phases of alumina was observed by XRD on spectra as verified by the data in literature [40]. XRD patterns of the nanocomposites having 0, 5, and 10 phr nano-Al_2O_3 showed a strong peak about $2\theta = 20°$. This peak is devoted to the amorphous structure of epoxy as previously reported in the literatures [41,42]. The value of d spacing for the various samples was almost similar but the peak intensity increased by the nanofiller concentration. The main peaks of the nano-Al_2O_3 in 2θ range of 30–50 were approximately disappeared at low concentrations of the nanofiller due to the reliable dispersion. But, at high concentration of 10%, we observed a few small peaks in the same 2θ range.

It could be implied that the quality of dispersion at high concentration was not excellent possibly owing to the nano-Al_2O_3 aggregation. Anyways, the crystalinity characteristics of the nanocomposites were influenced by the amount of the nanofiller.

To obtain further insights about the morphology of the produced thermosets we attempted to do SEM tests. SEM images on the fracture surface of the GDE/DGA system and its nanocomposite were depicted in Fig. 9.

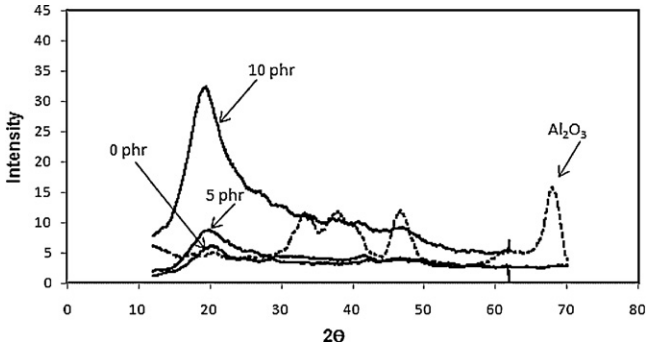

Fig. 8. XRD patterns of GDE/DGA/nanoalumina nanocomposite with nanoalumina content of 0, 5, and 10 phr and pure nanoalumina.

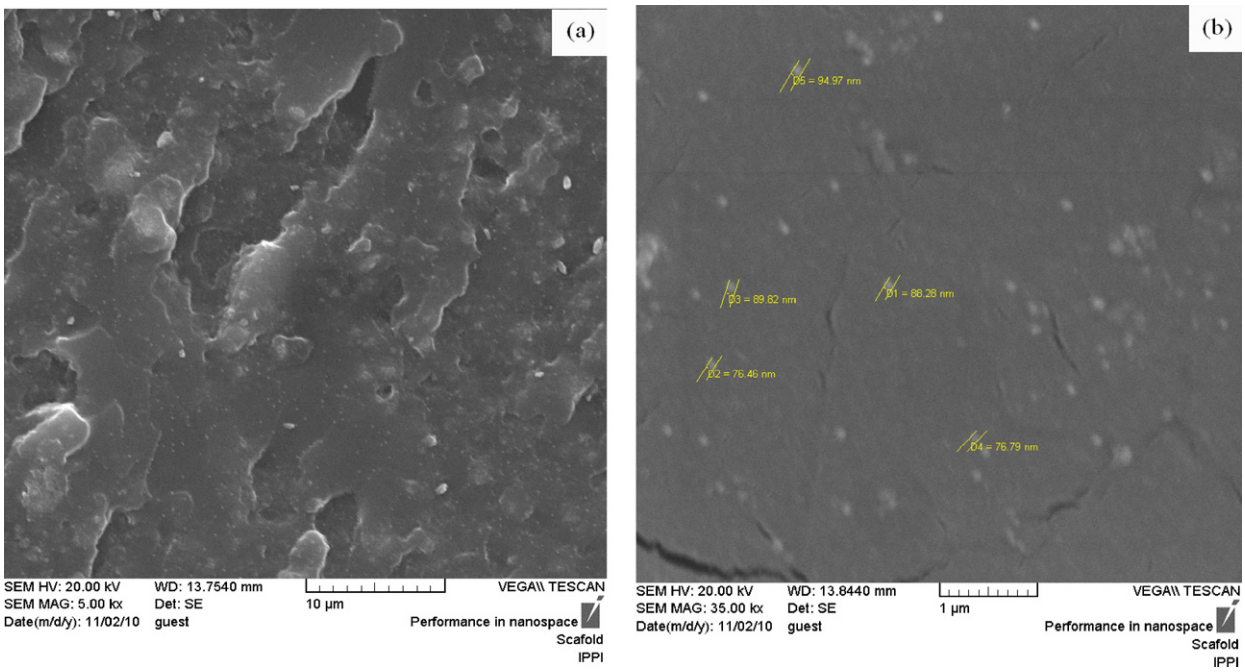

Fig. 9. Scanning electron micrographs on fracture surface of GDE/DGA/nanoalumina (10 phr) system (a and b).

SEM images revealed that the neat GDE system exhibits smooth and featureless on the surface, representing brittle failure of homogeneous materials with poor roughness whereas the rough surfaces of nanocomposite having 10 phr nano-Al_2O_3 are clearly indicative of GDE modification with the nanofiller. SEM images of GDE/DGA/nano-Al_2O_3 nanocomposite showed a homogenous dispersion of nano-Al_2O_3 in the GDE matrix at nanoscale level but some aggregates was also seen. From the SEM images, it might be implied that there is a good adhesion between the used nanofiller and GDE matrix. Therefore, the combination of better dispersion and adhesion of GDE/DGA/nano-Al_2O_3 nanocomposite probably will have contribution to its mechanical properties. The white zones on the SEM images are assigned to the nanofiller. The diameter of the white spots lies between 80 and 200 nm.

3.6. Thermal stability assessment

To evaluate thermal stability of the produced materials, TGA experiment was carried out on pure nanoalumina, GDE/DGA system, and GDE/DGA/nano-Al_2O_3 nanocomposite. The samples were cured isothermally at 130 °C for 4 h. TGA curves of the three samples are shown in Fig. 10. As expected, the nanofiller were stable well until 700 °C and a small amount of the observed mass loss could be assigned to the sample humidity. The neat GDE system and its nanocomposite showed a two step thermal degradation pattern. Apparently, the presence of the nanoalumina filler has a relatively minor effect on the first stage of thermal degradation owing to the same degradation onset. However, charring of the epoxy nanocomposite in the second degradation step takes place, in nitrogen, at a higher yield (ca. 8% at 700 °C) than the neat GDE system.

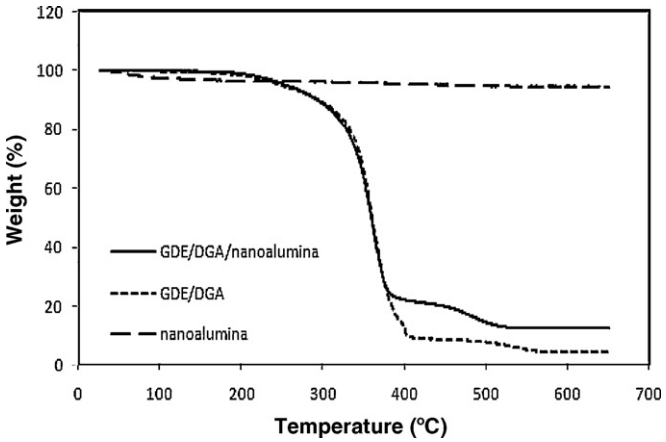

Fig. 10. TG curves of three system at heating rate of 10 °C/min.

4. Conclusions

The cure behavior of a novel nanocomposite based on glycerol diglycidyl ether was investigated by DSC. The experiments were applied in isothermal and nonisothermal modes. Basically, the data from kinetic analysis provides information on GDE state of cure which is important during processing of the nanocomposites. Under isothermal condition, the Kamal and Horie models were used to estimate the kinetic parameters. Our results showed that the Horie model is preferable in terms of better fitting of the experimental data. Model independent values of the global activation energy were calculated for the GDE nanocomposite using the Flynn–Wall–Ozawa isoconversional method and compared to the data obtained by the Vyazovkin advanced isoconversional approach. The both methods exhibited a same trend in activation energy changes. The Vyazovkin method was used to predict the times to reach practically complete cure at isothermal mode by the activation energies from the isoconversional approaches. The findings from morphology studies by XRD and SEM indicated that incorporation of nanoalumina into GDE matrix could be achieved homogeneously at nanoscale level. TGA result of GDE/DGA/nanoalumina (10%) sample showed about 8% increase in residue at 700 °C verifying that the thermal stability of the nanocomposite is better than that of the neat GDE system.

References

[1] A.M. Nucci, A. Nicolau, E.M.A. Mrtini, D. Samios, Eur. Polym. J. 42 (2006) 195–202.

[2] A. Nicolau, A.M. Nucci, E.M.A. Martini, D. Samios, Eur. Polym. J. 43 (2007) 2708–2717.
[3] P. Guerrero, K. De Caba, A. Valea, M.A. Corcuera, I. Mondragon, Polymer 37 (1996) 2195–2200.
[4] K. Hakala, R. Vatanparast, C. Li, S.Y. Peinado, P. Bosch, F. Catalina, Macromolecules (33) (2000) 5954–5959.
[5] B. Ellis, Chemistry and technology of epoxy resins, Blakie Academic Professionals, Glasgow, 1993.
[6] V.K. Srivastava, H. Kawada, Comp. Sci. Technol. 61 (2001) 2393–2403.
[7] A. Godara, D. Raabe, Comp. Sci. Technol. 67 (2007) 2417–2427.
[8] D. Bachtiar, S.M. Sapuan, M.M. Hamdan, Mater. Design 29 (2008) 1285–1290.
[9] M. Grujicic, W.C. Bell, L.L. Thompson, K.L. Koudela, B.A. Cheeseman, Mater. Sci. Eng. A 479 (2008) 10–22.
[10] S. Katz, E. Zaretsky, E. Grossman, H.D. Wagner, Comp. Sci. Technol. 69 (2009) 1250–1255.
[11] R.B. Yallee, R.J. Young, Composites Part A (29A) (1998) 1353–1362.
[12] S.C. Kwon, T. Adachi, W. Araki, A. Yamaji, Acta Mater. 54 (2006) 3369–3374.
[13] Y. Zheng, L. Cui, J. Schrooten, Mater. Lett. 59 (2005) 3287–3290.
[14] H. Miyagawa, M.J. Rich, L.T. Drzal, Thermochim. Acta 442 (2006) 67–73.
[15] Ch. Ma, Y. Chang, W. Ye, L. Duan, Ch. Wang, J. Supercrit. Fluid 45 (2008) 112–120.
[16] M.Z. Kassaee, F. Buazar, J. Manuf. Process 11 (2009) 31–37.
[17] A. Omrani, A.A. Rostami, M. Ghaemy, J. Appl. Polym. Sci. 101 (2006) 1257–1265.
[18] S.R.V. Castiglia, D. Fioretto, L. Verdini, D. Samios, J. Polym. Sci. Part B 39 (2001) 1326–1336.
[19] S. Li, E. Vuorimaa, H. Lemmetyinen, J. Appl. Polym. Sci. 81 (2001) 1474–1480.
[20] M. Abdalla, D. Dean, P. Robinson, E. Nyairo, Polymer 49 (2008) 3310–3317.
[21] K. Yang, M. Gu, Y. Jin, J. Appl. Polym. Sci. 110 (2008) 2980–2988.
[22] A. Allaoui, N.E. Bounia, Exp. Polym. Lett. 3 (2009) 588–594.
[23] A. Visco, L. Calabrese, C. Milone, J. Reinf. Plast. Comp. 28 (2009) 937–949.
[24] A. Omrani, A.A. Rostami, E. Sedaghat, Thermochim. Acta 497 (2010) 21–26.
[25] A. Omrani, L.C. Simon, A.A. Rostami, M. Ghaemy, Eur. Polym. J. 44 (2008) 769–779.
[26] M. Ghaemy, A.A. Rostami, A. Omrani, Polym. Int. 55 (2006) 279–284.
[27] M. Harsch, J.K. Kocsis, M. Holst, Eur. Polym. J. 43 (2007) 1168–1178.
[28] M. Ghaemy, A. Omrani, A.A. Rostami, J. Appl. Polym. Sci. 98 (2005) 1540–1547.
[29] S. Vyazovkin, N. Sbirrazzuoli, Macromolecules 29 (1996) 1867–1873.
[30] S. Vyazovkin, W. Linert, Chem. Phys. 193 (1995) 109–118.
[31] J.H. Flynn, L.A. Wall, J. Res. Nat. Bur. Standards (70A) (1966) 487–523.
[32] T. Ozawa, Bull. Chem. Soc. Jpn 38 (1965) 1881–1886.
[33] H. Stutz, J. Mertes, K. Neubecker, J. Polym. Sci. A 31 (1993) 1879–1886.
[34] S. Vyazovkin, J. Comput. Chem. 22 (2001) 178–183.
[35] N. Sbirrazzuoli, S. Vyazovkin, Thermochim. Acta 388 (2002) 289–298.
[36] S. Vyazovkin, N. Sbirrazzuoli, Macromol. Rapid Commun. 27 (2006) 1515–1532.
[37] S. Vyazovkin, D. Dollimore, J. Chem. Inf. Comp. Sci. 36 (1996) 42–45.
[38] G.I. Senum, R.T. Yang, J. Therm. Anal. 11 (1977) 445–447.
[39] S. Vyazovkin, Int. J. Chem. Kinet. 28 (1996) 95–101.
[40] Y.C. Sharma, V. Srivastava, A.K. Mukherjee, J. Chem. Eng. Data 55 (2010) 2390–2398.
[41] G. Malucelli, R. Bongiovanni, M. Sangermano, S. Ronchetti, A. Priola, Polymer 48 (2007) 7000–7007.
[42] L. Cheng, L. Zheng, G. Li, J. Zeng, Q. Yin, Physica B 403 (2008) 2584–2589.